1-1-2005

Evidence for the regulatory role of the N-terminal helix of secretory phospholipase A(2) from studies on native and chimeric proteins

Shan Qin
University of Central Florida

Abhay H. Pande
University of Central Florida

Kathleen N. Nemec
University of Central Florida

Xiaomei He
University of Central Florida

Suren A. Tatulian
University of Central Florida

THE JOURNAL OF BIOLOGICAL CHEMISTRY VOL. 280, NO. 44, pp. 36773–36783, November 4, 2005

Evidence for the Regulatory Role of the N-terminal Helix of Secretory Phospholipase A_2 from Studies on Native and Chimeric Proteins*

Received for publication, June 22, 2005, and in revised form, August 4, 2005 Published, JBC Papers in Press, August 15, 2005, DOI 10.1074/jbc.M506789200

Shan Qin[‡§], Abhay H. Pande[‡], Kathleen N. Nemec[‡], Xiaomei He[‡¶], and Suren A. Tatulian[‡1]

From the [‡]Biomolecular Science Center, University of Central Florida, Orlando, Florida 32826, the [§]Department of Molecular Biology, Massachusetts General Hospital, Harvard Medical School, Boston, Massachusetts 02114, and the [¶]Department of Chemistry, University of Central Florida, Orlando, Florida 32816

The phospholipase A_2 (PLA_2) enzymes are activated by binding to phospholipid membranes. Although the N-terminal α-helix of group I/II PLA_2s plays an important role in the productive mode membrane binding of the enzymes, its role in the structural aspects of membrane-induced activation of PLA_2s is not well understood. In order to elucidate membrane-induced conformational changes in the N-terminal helix and in the rest of the PLA_2, we have created semisynthetic human group IB PLA_2 in which the N-terminal decapeptide is joined with the ^{13}C-labeled fragment, as well as a chimeric protein containing the N-terminal decapeptide from human group IIA PLA_2 joined with a ^{13}C-labeled fragment of group IB PLA_2. Infrared spectral resolution of the unlabeled and ^{13}C-labeled segments suggests that the N-terminal helix of membrane-bound IB PLA_2 has a more rigid structure than the other helices. On the other hand, the overall structure of the chimeric PLA_2 is more rigid than that of the IB PLA_2, but the N-terminal helix is more flexible. A combination of homology modeling and polarized infrared spectroscopy provides the structure of membrane-bound chimeric PLA_2, which demonstrates remarkable similarity but also distinct differences compared with that of IB PLA_2. Correlation is delineated between structural and membrane binding properties of PLA_2s and their N-terminal helices. Altogether, the data provide evidence that the N-terminal helix of group I/II PLA_2s acts as a regulatory domain that mediates interfacial activation of these enzymes.

Enzymes of the phospholipase A_2 (PLA_2)[2] family hydrolyze the *sn*-2 ester bond of diacylglycerophospholipids and thus initiate the biosynthesis of lipid-derived mediators, such as eicosanoids and platelet-activating factor, which are potent mediators of inflammation, allergy, and tumorigenesis (1–3). These enzymes are divided into several groups and subgroups based on their amino acid sequences, tissue distribution, and functional features (1, 2).

PLA_2s gain their full activity only when they bind to phospholipid micelles or membranes, an effect known as interfacial activation (4–6). The molecular mechanism of interfacial activation has been the subject of debate over several decades. Initially, similarities of crystal structures of PLA_2s with and without bound substrate mimics argued against conformational changes in the enzymes during interfacial activation (4). Later, the interfacially activated form of group IB PLA_2 was modeled by anion-mediated dimers (7), which revealed significant conformational changes compared with "inactive" monomeric forms, mainly involving the loop that has the functionally important Tyr^{69}, and the presence of an assisting water molecule (8). Several spectroscopic studies also identified conformational changes in group IB and IIA PLA_2s upon binding to phospholipid micelles or membranes. Fluorescence studies indicated that the N-terminal helix of porcine group IB PLA_2 becomes rigid upon enzyme-substrate complex formation at the membrane surface (9, 10). This was confirmed by NMR experiments, which indicated that the N-terminal α-helix and H-bonded catalytically important residues of porcine group IB PLA_2 were flexible in the aqueous buffer and adopted a fixed conformation in a ternary complex of the enzyme with a substrate analog and phospholipid micelles (11, 12). Stabilization of the structure of membrane-bound human group IB was identified by Fourier transform infrared (FTIR) spectroscopy (13). In contrast, NMR and FTIR data have indicated that group IIA PLA_2s are characterized with stable secondary structure free in solution, including the N-terminal helix, and membrane binding of these enzymes is accompanied with destabilization of α-helices (14–17).

Previously, we have shown that deletion of the N-terminal α-helix of human IB PLA_2 results in a loss of the productive mode membrane binding capability and a 100-fold inhibition of the enzyme activity (13). Thus, experimental evidence accumulated to date suggests that the N-terminal α-helix of group I/II PLA_2s is a crucial structural domain necessary for a productive mode membrane binding and activity of the enzymes (13), conformational changes do occur in these enzymes during interfacial activation involving the N-terminal helix, and these conformational changes are group-specific. In order to understand the significance of differences in membrane-induced conformational changes in group I and II PLA_2s and the role of the N-terminal helix, it is important to examine the structural and functional effects of replacement of the N-terminal helix between PLA_2 isoforms. In this work, we present our findings on the effects of substitution of the N-terminal helix of human group IB PLA_2 (hIBPLA$_2$) by that of human group IIA PLA_2 (hIIAPLA$_2$) on the enzyme activity, membrane binding strength, membrane-induced conformational changes, and the precise mode of membrane binding. In order to monitor structural changes in individual

* This work was supported by NHLBI Grant HL65524 from the National Institutes of Health. The costs of publication of this article were defrayed in part by the payment of page charges. This article must therefore be hereby marked "*advertisement*" in accordance with 18 U.S.C. Section 1734 solely to indicate this fact.

[1] To whom correspondence should be addressed: Biomolecular Science Center, University of Central Florida, 12722 Research Pkwy., Orlando, FL 32826. Fax: 407-384-2062; E-mail: statulia@mail.ucf.edu.

[2] The abbreviations used are: PLA_2, phospholipase A_2; ATR-FTIR, attenuated total reflection Fourier transform infrared; DHTPC, diheptanoyl-thio-phosphatidylcholine; ΔN10, fragment of group IB phospholipase A_2 that lacks the first 10 residues; FPE, *N*-(fluorescein-5-thiocarbamoyl)-1,2-dihexadecanoyl-*sn*-glycero-3-phosphoethanolamine; FTIR, Fourier transform infrared; hIBPLA$_2$, human group IB phospholipase A_2; hIIAPLA$_2$, human group IIA phospholipase A_2; HX, hydrogen-deuterium exchange; N10hIB, N-terminal decapeptide of human group IB phospholipase A_2; N10hIIA, N-terminal decapeptide of human group IIA phospholipase A_2; N10IIA/IB PLA_2, phospholipase A_2 comprising the ten N-terminal residues of human group IIA isoform and the rest (residues 11–126) of human group IB isoform; POPC, 1-palmitoyl-2-oleoyl-*sn*-glycero-3-phosphocholine; POPG, 1-palmitoyl-2-oleoyl-*sn*-glycero-3-phosphoglycerol.

helical segments of the protein, we have chemically ligated unlabeled synthetic decapeptides corresponding to the N-terminal helix of either IB or IIA PLA_2s with the uniformly ^{13}C-labeled fragment of $hIBPLA_2$ that lacks the first 10 residues, and we used the semisynthetic, segmentally ^{13}C-labeled proteins to assess site-specific conformational effects upon membrane binding. Segmental isotope labeling also allowed determination of the angular orientation of membrane-bound proteins by polarized attenuated total reflection Fourier transform infrared (ATR-FTIR) spectroscopy. Observed conformational differences in the N-terminal and internal helices of $hIBPLA_2$ and of the chimeric PLA_2 (N10IIA/IB) containing the first 10 residues of $hIIAPLA_2$ and the rest from $hIBPLA_2$ indicate an important role for the N-terminal helix as a domain that regulates structural transformations during interfacial activation and facilitates proper membrane binding of group I/II PLA_2s.

EXPERIMENTAL PROCEDURES

Materials—The lipids 1-palmitoyl-2-oleoyl-*sn*-glycero-3-phosphocholine (POPC) and 1-palmitoyl-2-oleoyl-*sn*-glycero-3-phosphoglycerol (POPG) were purchased from Avanti Polar Lipids (Alabaster, AL). *N*-(Fluorescein-5-thiocarbamoyl)-1,2-dihexadecanoyl-*sn*-glycero-3-phosphoethanolamine (FPE) was from Invitrogen. The N-terminal decapeptides of $hIBPLA_2$ and $hIIAPLA_2$, Ac-Ala-Val-Trp-Gln-Phe-Arg-Lys-Met-Ile-Lys-NH_2 (N10hIB) and Ac-Asn-Leu-Val-Asn-Phe-His-Arg-Met-Ile-Lys-NH_2 (N10hIIA), respectively, were synthesized by Advanced ChemTech (Louisville, KY) and were ≥99% pure, as confirmed by high pressure liquid chromatography and mass spectrometry. C-terminally thioesterified peptides, containing a $-COSCH_2COOH$ group at the C terminus, were synthesized by SynPep Corp. (Dublin, CA) and were 99% pure. Most of other chemicals were purchased from Sigma.

Production of Recombinant and Semisynthetic Proteins—The semisynthetic, segmentally ^{13}C-labeled $hIBPLA_2$ was produced as described previously (18). Briefly, the plasmid for the PLA_2 fragment ΔN10 that lacks the first 10 residues was constructed by using a human pancreatic cDNA library, and the uniformly ^{13}C-labeled ΔN10 was expressed in *Escherichia coli* BL21(DE3) in an M9 minimal medium using $^{13}C_6$-D-glucose as a single metabolic source of carbon. The ΔN10 fragment was purified by ion exchange and size exclusion columns, as described (18). The C-terminally thioesterified N-terminal decapeptide N10hIB was ligated with the N-terminal cysteine of the ΔN10 fragment, followed by refolding of the ligated PLA_2 by dialysis against 25 mM Tris-HCl, 5 mM $CaCl_2$, 5 mM L-cysteine, 0.9 M guanidinium HCl (pH 8.0), and purified by using an ion exchange Mono Q 5/50 column. The chimeric, segmentally ^{13}C-labeled N10IIA/IB PLA_2 was produced in a similar manner except that the thioesterified N10hIIA peptide was used for chemical ligation. In both cases, the ligation reaction was allowed to proceed for 6 h at 37 °C. The ligated protein was separated from the unligated peptide and the ΔN10 fragment by an ion exchange Mono Q column. The profile of elution of the chimeric PLA_2 sample from the Mono Q column showed two major protein peaks (Fig. 1*A*), one of which was identified as the chimeric PLA_2 and the other as the unligated ΔN10 fragment (the peptide was eluted before the ligated PLA_2). Analysis of the elution peaks by SDS-PAGE showed that the chimeric PLA_2 was purified to homogeneity (Fig. 1*B*). The prokaryotic expression vector with the inserted $hIIAPLA_2$ gene that incorporates an N1A mutation was kindly provided by Prof. David Wilton (University of Southampton, UK). Expression and purification of $hIIAPLA_2$ were conducted as described (19), except the purification by a heparin column was followed by additional purification using a size exclusion HiLoad Superdex 75 column, which yielded highly pure and active enzyme.

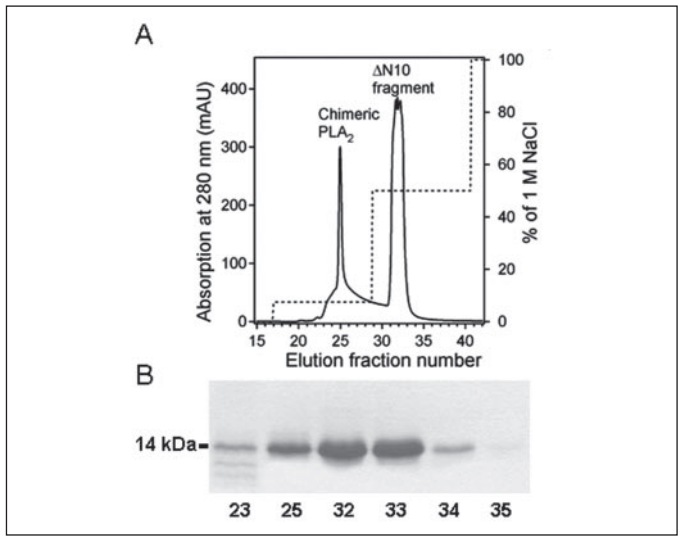

FIGURE 1. **Purification of the semisynthetic, segmentally ^{13}C-labeled chimeric PLA_2 by ion exchange chromatography.** The thioesterified decapeptide Asn-Leu-Val-Asn-Phe-His-Arg-Met-Ile-Lys-NH_2-$COSCH_2COOH$ was ligated with the ^{13}C-labeled fragment ΔN10 in a buffer containing 6 M guanidinum-HCl, 100 mM sodium phosphate, 5% β-mercaptoethanol, 1 mM EDTA, 4% thiophenol, and 4% benzyl mercaptan, pH 7.4. The concentrations of the ΔN10 fragment and the peptide were 16 and 1.6 mg/ml, respectively. The reaction was allowed to proceed for 6 h at 37 °C, followed by refolding of the ligated protein and purification using ion exchange Mono Q 5/50 column chromatography. *A,* the elution profile of the sample from the Mono Q column (*continuous line, left axis*). The initial buffer was 20 mM Tris-HCl (pH 9.0). Elution was conducted with a stepwise increase of NaCl concentration in the same buffer (*broken line, right axis*), and 0.5-ml fractions were collected. The peak at fraction number 25 was the ligated product, *i.e.* the chimeric PLA_2, as confirmed by its molecular mass, high PLA_2 activity, and spectroscopic data, whereas the peak at fraction number 32 was the unligated ^{13}C-labeled ΔN10 fragment. The free peptide eluted before the chimeric PLA_2. *B,* Coomassie-stained SDS gel of elution fractions shown in *A*. The single band corresponding to fraction 25 shows that the ligated chimeric PLA_2 was isolated as a pure protein.

PLA_2 Activity Assay—PLA_2 activity was measured using an $sPLA_2$ activity kit from Cayman Chemical (Ann Arbor, MI), as described (13). The assay buffer contained 100 mM KCl, 10 mM $CaCl_2$, 0.3 mM Triton X-100, 1 mg/ml bovine serum albumin, 25 mM Tris-HCl (pH 7.5), 0.4 mM 5,5′-dithio-*bis*-(2-nitrobenzoic acid), and 1.5 mM diheptanoyl-thiophosphatidylcholine (DHTPC) as a PLA_2 substrate. The sample was contained in a 0.4-cm optical path length rectangular quartz cuvette. The reaction was initiated by adding 3 μl of a 67 μg/ml PLA_2 solution to a final PLA_2 concentration of 1.0 μg/ml, and the enzyme activity was monitored by an increase in absorption at 414 nm due to PLA_2-catalyzed cleavage of DHTPC, exposure of thiol groups, and monomerization of 5,5′-dithio-*bis*-(2-nitrobenzoic acid). A Cary 100 double-beam spectrophotometer (Varian Inc., Palo Alto, CA) was used. The specific activity (v_o) of PLA_2 was calculated based on the initial slope of the time dependence of absorption at 414 nm, using an extinction coefficient of $\epsilon_{414} = 13{,}600\ M^{-1}\ cm^{-1}$ for 5-thionitrobenzoic acid.

Fluorescence and Circular Dichroism Experiments—Fluorescence and CD measurements were conducted using a Jasco 810 spectrofluoropolarimeter (Jasco Corp., Tokyo, Japan), as described previously (13). This particular model is designed for CD experiments and is equipped with an additional photomultiplier tube mounted at 90° for fluorescence measurements, as well as with a Peltier temperature controller. Fluorescence experiments were carried out on samples in 100 mM NaCl, 1 mM NaN_3, and 50 mM Hepes (pH 7.4) contained in a rectangular 0.4-cm optical path length quartz cuvette, at 22 °C, using excitation and emission slits of 4 and 10 nm, respectively. For CD experiments, the proteins were dissolved in a 10 mM sodium phosphate buffer, pH 7.4, and measurements were conducted using a 0.5-mm optical path length quartz cuvette. In both fluorescence and CD experiments, five

scans were averaged, and the spectra were corrected by subtracting the spectra of blank buffers.

Membrane Binding Experiments—In order to measure the binding to phospholipid membranes of the N10IIA/IB chimeric PLA_2, as well as of group IB and IIA PLA_2s and their N-terminal decapeptides, fluorescence spectroscopy was used. The conventional resonance energy transfer technique could not be used because some molecules did not have tryptophan (the N10IIA/IB and hIIAPLA$_2$) and some did not have any fluorophores at all (the N10hIIA peptide). Instead, the increase in fluorescence emission intensity of FPE in vesicle membranes upon protein or peptide binding was used, as described before (20, 21). FPE was incorporated at 2 mol % in large unilamellar phospholipid vesicles, which were prepared by extrusion through 100-nm pore size polycarbonate membranes, as described (13). The buffer was 10 mM Hepes, 1 mM NaN_3, 1 mM EGTA (pH 7.4), and fluorescence experiments were conducted as described above. Excitation was at 490 nm, and emission spectra were recorded between 502 and 540 nm at 22 °C. After recording an initial spectrum of vesicles in the buffer, proteins or peptides were added to the lipid suspension at increasing concentrations from a stock solution, and consecutive fluorescence emission spectra were recorded following equilibration of the sample for 2 min, with constant stirring. The fluorescence intensity of FPE is sensitive to the ionization state of the carboxyl group of fluorescein; the emission intensity increases with increasing deprotonation. The fluorescein moiety of FPE is located at the interface of the negatively charged membrane, where the local environment is more acidic than the bulk phase because of electrostatic attraction of protons to the membrane. This causes partial protonation of the carboxyl group of fluorescein, resulting in a moderate level of fluorescence intensity. Adsorption of cationic protein or peptide molecules to the membrane reduces the negative surface charge of the membrane, which results in a protein (or peptide) dose-dependent deprotonation of fluorescein and an increase in the fluorescence intensity. This effect was used to measure binding isotherms for PLA_2s and their N-terminal peptides.

Analysis of Membrane Binding Data—Binding of proteins and peptides to membranes was analyzed using a logic described earlier (13). The protein is added to preformed lipid vesicles, resulting in binding of the protein to the external surface of vesicles. If one considers that only a fraction δ of the total lipid is accessible to the protein, and the binding of each protein molecule makes N lipid molecules inaccessible for other proteins, then the dissociation constant of the binding process can be presented as shown in Equation 1,

$$K_D = \frac{([P]-[P]_b)(\delta[L]-N[P]_b)}{N[P]_b} \qquad \text{(Eq. 1)}$$

where $[P]$ and $[L]$ are the total concentrations of the protein and the lipid, respectively, and $[P]_b$ is the concentration of the membrane-bound protein. When the lipid fluorescence is monitored as the lipid is being titrated with the protein, the relative change in the fluorescence signal is as shown in Equation 2,

$$\frac{\Delta F}{\Delta F_{max}} = \frac{[L]_b}{\delta[L]} \qquad \text{(Eq. 2)}$$

where ΔF is the change in fluorescence intensity at a given protein concentration; ΔF_{max} is the saturating level of ΔF at high protein concentration, and $[L]_b$ is the concentration of protein-bound lipid. We have used ΔF values at 518 nm. Using $[P]_b = [L]_b/N = \Delta F_{rel}\delta[L]/N$ (where $\Delta F_{rel} \equiv \Delta F/\Delta F_{max}$), we convert Equation 1 into a quadratic equation with respect to ΔF_{rel} and solve it as shown in Equations 3 and 4,

$$\Delta F_{rel} = a - \sqrt{a^2 - \frac{N[P]}{\delta[L]}} \qquad \text{(Eq. 3)}$$

where

$$a = \frac{1}{2}\left(\frac{N(K_D + [P])}{\delta[L]} + 1\right) \qquad \text{(Eq. 4)}$$

The plus sign in front of the square root is useless because it results in values of $\Delta F_{rel} > 1$. It is seen from Equation 1 that at half-saturation of protein binding, when $\Delta F_{rel} = 0.5$ (Equation 5),

$$K_D = [P]_{1/2} - \frac{\delta[L]}{2N} \qquad \text{(Eq. 5)}$$

where $[P]_{1/2}$ is the protein concentration corresponding to $\Delta F_{rel} = 0.5$.

Changes in FPE fluorescence intensity, ΔF, were measured at various protein concentrations, $[P]$, and ΔF values were plotted against $\Delta F/[P]$. These linear (Scatchard) plots were used to evaluate ΔF_{max} and $[P]_{1/2}$ from the extrapolated intercept with the ΔF axis and from the slope, respectively. Experimental binding isotherms were constructed by plotting $\Delta F/\Delta F_{max}$ against $[P]$. The theoretical isotherms were simulated through Equation 3 using K_D and N as fitting parameters. Despite two fitting parameters, determination of both K_D and N by this method is reliable. In Equation 5, $[P]_{1/2}$ can be determined using the experimental data, as described above, and δ is 0.52 for vesicles 100 nm in diameter, with a membrane thickness of 4 nm (13). Replacement of K_D in Equation 4 by the expression in equation 5 yields an equation with only one unknown, *i.e. N*. Hence, fitting of the experimental curves can be done by varying N in a physically reasonable range, and once a best fit is achieved, the K_D value can be calculated through Equation 5 by using the best fit value of N. The Gibbs free energies of membrane binding, ΔG_b, were calculated using dissociation constants, as described (13).

Attenuated Total Reflection FTIR Experiments—Polarized ATR-FTIR experiments were carried out using a Vector 22 FTIR spectrometer (Bruker Optics, Billerica, MA), as described previously (13). A model 611 Langmuir-Blodgett trough (Nima, Coventry, UK) was used to deposit a POPC monolayer on a germanium internal reflection plate $0.1 \times 2 \times 5$ cm^3 in size and with 45° angles (Spectral Systems, Irvington, NY), followed by injection of sonicated vesicles composed of 80 mol % POPC and 20 mol % POPG and formation of supported phospholipid membranes. The protein or the peptide was dissolved in an H_2O-based buffer consisting of 100 mM NaCl, 1 mM NaN_3, 1 mM EGTA, 50 mM Hepes (pH 7.4) and was injected into the ATR cell that contained the supported membrane. After allowing the protein to bind to the membrane (~15 min), the cell was gently flushed with a ^2H_2O-based buffer of the same composition, followed by recording a series of spectra at alternating parallel and perpendicular polarizations of the incident infrared light, at 2 cm^{-1} resolution. The polarized spectra were used for two purposes. First, the spectra measured at parallel and perpendicular polarization were used to create "corrected" spectra as $A_{corrected} = A_{\parallel} + 0.8A_{\perp}$, which were used for calculation of the second derivative spectra and evaluation of secondary structures of proteins, as described before (13, 22). Second, the polarized spectra were used to evaluate the linear dichroic ratios and molecular orientation with respect to the membrane normal, as described (13, 23). Simulation of second derivatives was accompanied with 13-point Savitzky-Golay smoothing in order to avoid amplification of high frequency noise. Amide I components were

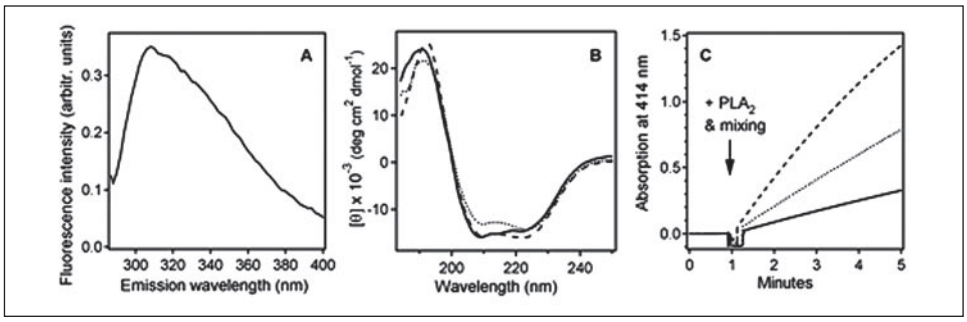

FIGURE 2. **Initial structure-function characterization of the chimeric N10IIA/IB PLA_2.** *A,* fluorescence spectrum of the semisynthetic chimeric PLA_2 in a buffer containing 100 mM NaCl, 1 mM NaN_3, and 50 mM Hepes (pH 7.4), in a 0.4-cm optical path length quartz cuvette. Excitation was at 275 nm, and the emission peak was located at 308 nm, characteristic of tyrosine fluorescence of a folded, tryptophan-less protein. *B,* circular dichroism spectra of the recombinant $hIBPLA_2$ (*dotted line*), $hIIAPLA_2$ (*dashed line*), and of the semisynthetic chimeric PLA_2 (*continuous line*) in a buffer containing 10 mM sodium phosphate buffer, pH 7.4, in a 0.5-mm optical path length quartz cuvette. All three proteins contain ~40% α-helix, as judged from the ellipticity at 222 nm, but the shape of the spectrum of the chimeric protein suggests more rigid helices compared with those in $hIBPLA_2$ and $hIIAPLA_2$. *C,* activities of the recombinant $hIBPLA_2$ (*dotted line*), $hIIAPLA_2$ (*dashed line*), and the semisynthetic chimeric PLA_2 (*continuous line*) as measured in a buffer containing 100 mM KCl, 10 mM $CaCl_2$, 0.3 mM Triton X-100, 1 mg/ml bovine serum albumin, 25 mM Tris-HCl (pH 7.5), 0.4 mM 5,5′-dithio-bis-(2-nitrobenzoic acid), and 1.5 mM DHTPC as a substrate. PLA_2s were added to a final concentration of 1.0 μg/ml, followed by stirring for ~10–15 s and recording the absorption at 414 nm. The method is based on PLA_2-catalyzed cleavage of the *sn*-2 thioester bond of DHTPC, exposure of free thiol groups that cause monomerization of 5,5′-dithiobis(2-nitrobenzoic acid) resulting in characteristic absorption at 414 nm. The initial slopes of time dependence of absorption were used to estimate activities of PLA_2s. All measurements were conducted at 22 °C. See text for more details.

obtained by curve fitting, using the number and positions of the inverted second derivative peaks as input parameters. The results of curve fitting were considered satisfactory when the peak frequencies of all components were within a ± 1 cm^{-1} range compared with the input frequencies and when the sum of all components (the "curve fit") was practically identical to the measured spectrum.

Determination of the Orientation of Membrane-bound PLA_2—The orientation of membrane-bound chimeric N10IIA/IB PLA_2 was determined by polarized ATR-FTIR spectroscopy. First, the structure of the protein was modeled by Swiss-Model (24) using the structure of porcine pancreatic PLA_2 as a template (Protein Data Bank entry 1P2P). The modeled structure had three α-helices, which we call helix 1 (residues 1–10), 2 (residues 43–57), and 3 (91–108). The C-α atom coordinates were used to determine the orientations of all three α-helices of the protein relative to the "protein" coordinate system Σ_p with axes x^*, y^*, z^*, in which the coordinates are given, and the helical orientations were further used to determine all interhelical angles, using the analytical geometry algorithms described earlier (18). This indicated that the angle between the helices 2 and 3 was 6.2°, which allowed us to consider these two helices approximately parallel to each other and to use a common order parameter to describe their orientation with respect to the membrane. (When the N → C directionality of helices is considered, the interhelical angle would be 173.8°, but in terms of infrared order parameters, parallel and antiparallel helices are equivalent.) Polarized ATR-FTIR spectroscopy was used to measure the amide I bands of the membrane-bound, segmentally ^{13}C-labeled chimeric N10IIA/IB PLA_2 at parallel and perpendicular orientations of the infrared light. Spectral separation of the α-helical signals generated by the unlabeled N-terminal helix and the ^{13}C-labeled helices 2 and 3 allowed determination of two order parameters, one for the N-terminal helix and one for the helices 2 and 3. Knowledge of the orientations of the two helices in the protein coordinate system Σ_p and with respect to the membrane normal then allowed determination of the angles between the membrane normal and the three axes of the system Σ_p, using an algorithm described elsewhere (18). This provides the angular orientation of the protein molecule relative to the membrane.

An ideal way to position precisely the protein at the membrane surface is to determine the coordinates of the protein atoms in a "membrane" coordinate system, Σ_m, with axes *x, y,* and *z,* which has its *xy* plane in the membrane center, between the two lipid leaflets, and the *z* axis is perpendicular to the membrane surface. This was achieved as follows. The protein molecule was considered at an arbitrary rotation about the *z* axis, maintaining the angles between the *z* axis and the three axes of the protein system Σ_p, as determined above. This does not reduce the generality because the protein has an unrestricted rotational freedom about the *z* axis. This allows determination of all nine angles between the protein and membrane coordinate systems, using the laws of direction cosines, which in turn allows transformation of the protein atom coordinates from the system Σ_p to the system Σ_m.

RESULTS AND DISCUSSION

Initial Structure-Function Characterization of the Chimeric N10IIA/IB PLA_2—The initial structure-activity characterization of the chimeric N10IIA/IB PLA_2 involved fluorescence and CD experiments and an activity assay. The chimeric protein is devoid of tryptophans but contains nine tyrosines, hence its fluorescence spectrum was measured based on tyrosine emission. As shown in Fig. 2*A*, the protein had a fluorescence emission maximum around 308 nm when excited at 275 nm, which is close to the tyrosine emission peak at ~306 nm in folded proteins (13, 25, 26). Because fluorescence spectra provide little information on the secondary structure of proteins, we used CD spectroscopy to evaluate the secondary structure content in the chimeric N10IIA/IB PLA_2 and to compare it with that of the group IB and IIA PLA_2s. The CD spectrum of the N10IIA/IB PLA_2 demonstrated double minima around 208 and 222 nm, with an absolute value of the mean residue molar ellipticity at 222 nm ($[\theta]_{222}$) comparable with those measured for group IB and IIA PLA_2s (Fig. 2*B*). This indicates that the chimeric protein is folded into a structure that comprises ~40% α-helix, which is characteristic of group I/II PLA_2s (4, 5). The shape of the CD spectrum of the chimeric protein was different from those of the group IB and IIA PLA_2s, however. The CD spectrum of the N10IIA/IB PLA_2 exhibited an increased ellipticity ratio $[\theta]_{208}/[\theta]_{222}$ as compared with both $hIBPLA_2$ and $hIIAPLA_2$. Reduced values of the ellipticity ratio $[\theta]_{208}/[\theta]_{222}$ are associated with deviations of the α-helix structure from a standard, rigid helix geometry, *e.g.* by formation of coiled-coil structures (27, 28) or distorted helices (29). Although two internal α-helices of group I/II PLA_2s are nearly antiparallel and disulfide-bonded, they are not likely to form a coiled-coil structure (see below). The observed feature is therefore more likely to indicate a less flexible conformation of the chimeric PLA_2 compared with the $hIBPLA_2$ and $hIIAPLA_2$.

To assess the influence of the substitution of the N-terminal helix on PLA_2 activity, the activity of the chimeric PLA_2, as well as of $hIBPLA_2$

TABLE ONE

Parameters characterizing membrane binding of PLA_2s and N-terminal peptides

Values of pI and excess charge are calculated considering all cysteines are oxidized, with no account for the presence of Ca^{2+} in PLA_2 molecules because binding experiments were conducted in the presence of 1 mM EGTA.

Molecule	pI	Excess charge at pH 7.4	20% POPG			40% POPG		
			K_D	ΔG_b	N	K_D	ΔG_b	N
			μM	kcal/mol		μM	kcal/mol	
$hIBPLA_2$	9.29	+2.174	6.04	−9.49	36	1.44	−10.34	36
N10hIB	11.17	+2.998	2.50	−10.01	9	0.60	−10.86	9
$hIIAPLA_2$	10.76	+15.241	2.75	−9.96	36	0.30	−11.27	36
N10hIIA	11.0	+2.065	5.72	−9.52	9	2.50	−10.01	9
N10IIA/IB	8.98	+1.241	10.0	−9.19	36	1.80	−10.21	36

and $hIIAPLA_2$, was measured by using DHTPC micelles as substrate. The activity of the chimeric enzyme, as evaluated based on the initial slope of the time dependence of product accumulation, was $v_o = 9 \pm 2$ μmol/min/mg (Fig. 2*C*), which is considerably lower than the activities of $hIBPLA_2$ and $hIIAPLA_2$, 24 ± 5 and 52 ± 8 μmol/min/mg, respectively (shown are mean values and standard deviations from three experiments). Although $hIIAPLA_2$ shows little activity toward zwitterionic phosphatidylcholine membranes (30, 31), it is more active than $hIBPLA_2$ toward micelles of short chain DHTPC. A possible explanation of this is that the extremely high excess positive charge of $hIIAPLA_2$ (~15 excess cationic charges at pH 7.4, see TABLE ONE) prevents binding to zwitterionic membranes because of strong positive surface charge of membranes that rapidly builds up upon binding of a few PLA_2 molecules. Micelles, on the other hand, can afford binding of only one PLA_2 molecule at a time because of their small size, which precludes electrostatic repulsion effects. These data indicate that in addition to structural differences that are reflected in CD spectra, the chimeric enzyme has a specific activity severalfold lower compared with those of group IB and IIA enzymes.

The Structure of Membrane-bound Chimeric PLA_2 as Compared with That of the $hIBPLA_2$—As described in the Introduction in more detail, group IB PLA_2s have been shown to acquire a more rigid structure upon binding to phospholipid micelles or membranes, involving primarily the N-terminal α-helix (9–13), whereas membrane binding of group IIA PLA_2s results in more flexible α-helices (14–17). Because the N-terminal α-helix of group I/II PLA_2s is a crucial structural component of the membrane binding face of these enzymes, it is important to identify its contribution to changes in the secondary or dynamic structure of PLA_2s during membrane binding. In order to test the hypothesis that the N-terminal helix of membrane-bound $hIBPLA_2$ is rigid, but its substitution by the N-terminal helix from $hIIAPLA_2$ may impart flexibility to the enzyme, we studied the semisynthetic $hIBPLA_2$ in which an unlabeled N-terminal decapeptide was ligated with the ^{13}C-labeled fragment ΔN10, as well as a semisynthetic, segmentally ^{13}C-labeled chimeric N10IIA/IB PLA_2, by ATR-FTIR spectroscopy. The amide I spectra of segmentally ^{13}C-labeled proteins are broader and more complex than those of unlabeled proteins. Amide I components that represent certain secondary structure elements, some of which are ^{13}C-labeled and the others are not, undergo hydrogen-deuterium exchange (HX) with distinct rates, creating a dynamically transforming set of time-dependent spectra (Fig. 3). In addition, both labeled and unlabeled amide oscillators are involved in through-bond and through-space vibrational couplings with ^{12}C- or ^{13}C-oscillators, which affects the frequencies and intensities of amide I components in a complex way (32–35).

During the first 90 min of HX, the high frequency wing of the amide I band of membrane-bound, segmentally ^{13}C-labeled $hIBPLA_2$ shifts toward lower frequencies by ~20 cm^{-1} because of HX, whereas the low frequency wing undergoes a more moderate downshift (Fig. 3*A*). The second derivative spectra, which were used as a resolution enhancement tool, reveal at least 10 components between 1690 and 1570 cm^{-1} (Fig. 3*B*). A well defined amide I component at 1658 cm^{-1} is readily assigned to the unlabeled N-terminal α-helix of $hIBPLA_2$, whereas the components at 1619 and 1609 cm^{-1} are assigned to the unexchanged and exchanged ^{13}C-labeled helices of the protein, respectively (23, 32–38). The component at 1658 cm^{-1} undergoes slow HX, because it is only at ~15 min following exposure to ^2H_2O that spectral downshift of this component clearly manifests itself (Fig. 3*B*). On the other hand, the signal assigned to the ^{13}C-labeled helices 2 and 3 is split into components at 1619 and 1609 cm^{-1}, already at 1 min of exposure to ^2H_2O, and undergoes little spectral change thereafter. As seen from the unprocessed amide I spectra (Fig. 3*A*), during the course of HX absorption intensity migrates from the high to the low frequency region, which may partially compensate the decrease in the 1619 cm^{-1} component during HX. These spectral features thus may indicate an increased stability of the N-terminal α-helix of the $hIBPLA_2$ compared with the two internal helices.

The amide I bands of the membrane-bound segmentally ^{13}C-labeled chimeric N10IIA/IB PLA_2 are different from those of the $hIBPLA_2$ in terms of both the spectral line shape and the dynamics. The high frequency wing of the amide I band undergoes only an 8 cm^{-1} downshift in 90 min, and despite this, the peak of the amide I band is located at 1608–1604 cm^{-1} (Fig. 3*C*), which is ~12 cm^{-1} lower than the amide I peak of the $hIBPLA_2$ (Fig. 3*A*). These characteristics reflect the fact that the component corresponding to the N-terminal helix of the chimeric protein is still located at 1657 cm^{-1}, but the component corresponding to the ^{13}C-labeled helices 2 and 3 is shifted farther down to 1608–1604 cm^{-1}, as seen from the second derivative spectra of Fig. 3*D*. Moderate spectral shifts for a protein in ^2H_2O indicates an overall more rigid structure. The more rigid conformation of the chimeric PLA_2 agrees with the above conclusion deduced from CD data (Fig. 2*B*). Although both unlabeled and ^{13}C-labeled helices undergo gradual HX, resulting in time-dependent diminution of corresponding signals in the second derivative spectra (Fig. 3*D*), at 60–90 min following exposure to ^2H_2O there still is a major component around 1604 cm^{-1}, whereas the component around 1657 cm^{-1} nearly vanishes. This may result from faster HX of the N-terminal helix compared with the ^{13}C-labeled helices, which, in contrast to $hIBPLA_2$, is indicative of more stable internal helices of the chimeric PLA_2 compared with the N-terminal helix.

A possible interpretation of lower amide I frequency of the ^{13}C-labeled α-helices of the chimeric PLA_2 compared with $hIBPLA_2$ might be the formation of a double-stranded coiled-coil by the two internal helices of the chimeric PLA_2 and sequestered, rigid helices in the $hIBPLA_2$, because two-stranded coiled-coils are characterized by significantly lower amide I frequencies compared with standard α-helices (39, 40).

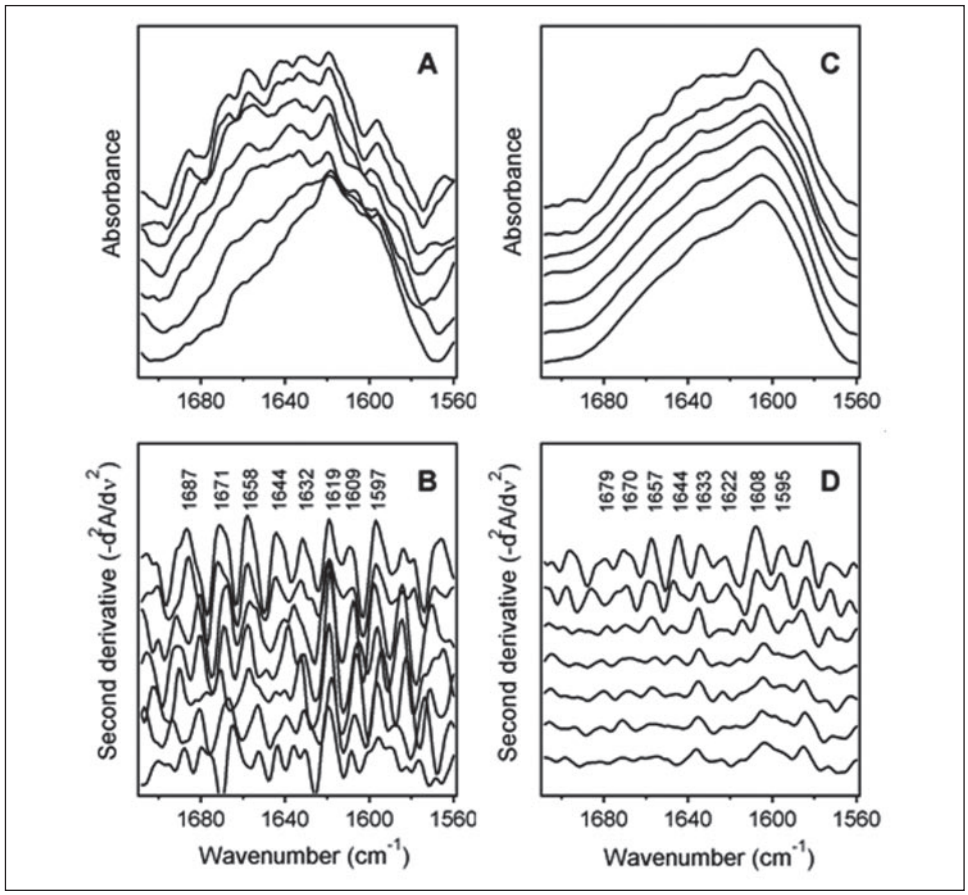

FIGURE 3. **Structural characterization of the semisynthetic, segmentally ^{13}C-labeled hIB-PLA_2 and the chimeric N10IIA/IB PLA_2 by ATR-FTIR spectroscopy.** *A,* ATR-FTIR amide I bands of the semisynthetic, segmentally ^{13}C-labeled hIB-PLA_2 bound to a phospholipid bilayer membrane supported on a germanium internal reflection plate. The membrane was composed of POPC in the lower leaflet (facing the plate) and POPC/POPG (4:1, mol/mol) in the upper leaflet. Initially the protein was dissolved in a buffer containing 100 mM NaCl, 1 mM NaN_3, 1 mM EGTA, 50 mM Hepes in H_2O (pH 7.4) and was injected to the ATR cell with the supported membrane. After binding of the protein to the membrane, the cell was flushed with a ^2H_2O-based buffer of the same composition, and spectra were recorded at parallel and perpendicular orientations of the infrared light. Presented here are the corrected and normalized spectra. They were obtained as $A_{corrected} = A_{\parallel} + 0.8A_{\perp}$, which are "polarization-independent" and therefore reflect the true secondary structural features of the protein, followed by normalization of the total integrated area to 1 absorbance unit/cm. The stacked spectra correspond to exposure of the protein to ^2H_2O for 1, 3, 7.5, 26, 44, 66, and 90 min (from *top* to *bottom*), which applies to all four panels. *B,* the second derivative amide I spectra derived from the spectra of *A*, accompanied with 13-point Savitzky-Golay smoothing. Here, as well as in *D*, the wave numbers of prominent amide I components are marked by vertically oriented numbers. *C,* ATR-FTIR spectra of the semisynthetic, segmentally ^{13}C-labeled chimeric N10IIA/IB PLA_2 bound to a supported membrane under identical conditions as in *A*. *D,* the second derivative spectra derived from spectra of *C*, accompanied with 13-point Savitzky-Golay smoothing.

However, this is not likely to be the case because the internal helices of group I/II PLA_2s are not long enough and lack heptad repeat features, which facilitate helical coiled-coil formation (41). A more substantiated interpretation is based on consideration of the relative amide I intensity and the spectral location of the ^{13}C-helices. The ratios of apparent extinction coefficient of ^{13}C-labeled and unlabeled helices of both the hIBPLA$_2$ and the chimeric PLA_2 were estimated as $\epsilon_{13C}/\epsilon_{12C} = I_{13C}n_{12C}/I_{12C}n_{13C}$, where I and n are the integrated amide I intensities and the numbers of amino acid residues for corresponding helices, respectively. The corrected, polarization-independent ATR-FTIR spectra were used for such analysis, which indicated that $\epsilon_{13C}/\epsilon_{12C} = 0.54$ for hIBPLA$_2$ and $\epsilon_{13C}/\epsilon_{12C} = 0.67$ for the chimeric protein. Increased absorptivity of the amide I mode of unlabeled *versus* ^{13}C-labeled helices was detected before for synthetic 32-mer peptides containing stretches of three consecutive ^{13}C-labeled residues (38). Our data indicate that the amide I absorptivity of the ^{13}C-labeled helices relative to the unlabeled helix is higher in the chimeric PLA_2 as compared with the hIB-PLA_2. On the other hand, the amide I peak of ^{13}C-labeled α-helices of the chimeric protein occurs at lower frequencies compared with the hIBPLA$_2$. Because several studies have indicated that temperature-induced destabilization of segmentally ^{13}C-labeled α-helical peptides was accompanied with a decrease in intensity and an increase in the frequency of both unlabeled and ^{13}C-labeled segments (38, 42, 43), these spectral features may be interpreted in terms of a more rigid structure for the internal helices of the chimeric protein compared with the IB PLA_2. In support of this conclusion, it is worth mentioning that α_{II}-helices, which are characterized by much weaker helical H-bonding and are more flexible than standard α_I-helices (44), generate amide I modes at 10–12 cm^{-1} higher frequencies compared with regular α-helices (45–47).

The lower relative amide I intensity of the unlabeled N-terminal helix of the N10IIA/IB PLA_2 as compared with that of hIBPLA$_2$ is consistent with a more flexible N-terminal helix in the chimeric protein. Although this latter inference would assume an upward spectral shift of the amide I signal of the N-terminal helix in the chimeric PLA_2 compared with that of hIBPLA$_2$, which has not been observed (both components occur at 1657–1658 cm^{-1}), still the most consistent conclusion from the CD and ATR-FTIR experiments is that the overall structure of the chimeric PLA_2 is more rigid than that of the hIBPLA$_2$, but in the chimeric protein the N-terminal helix is more flexible than the rest of the protein.

Membrane Binding of Group IB and IIA PLA_2s, Their N-terminal Peptides, and the Chimeric PLA_2—Membrane binding is a crucial determinant of PLA_2 activity. Because in this work we consider the structural and functional consequences of the substitution of the N-terminal helix of hIBPLA$_2$ by that of hIIAPLA$_2$, we have determined and compared membrane binding parameters of hIBPLA$_2$, hIIAPLA$_2$, their N-terminal peptides, and the chimeric N10IIA/IB PLA_2. Fig. 4*A* shows representative fluorescence spectra indicating a gradual increase in the emission intensity of FPE (2 mol % in membranes of large unilamellar vesicles) with increasing concentration of hIBPLA$_2$. The increments of fluorescence change at each protein concentration, ΔF, were corrected by taking into account the decrease in fluorescence intensity due to sample dilution (Fig. 4*B*) and were used to construct the binding isotherms (Fig. 4*C*), as described under "Experimental Procedures." The binding isotherms were described by Equations 3 and 4, and the dissociation constants (K_D) and the numbers of lipids per membrane-bound protein (N) were evaluated from the best fit between the experimental and simulated isotherms.

There is strong evidence that membrane binding of group I and II PLA_2s has a strong electrostatic component, resulting in poor binding to

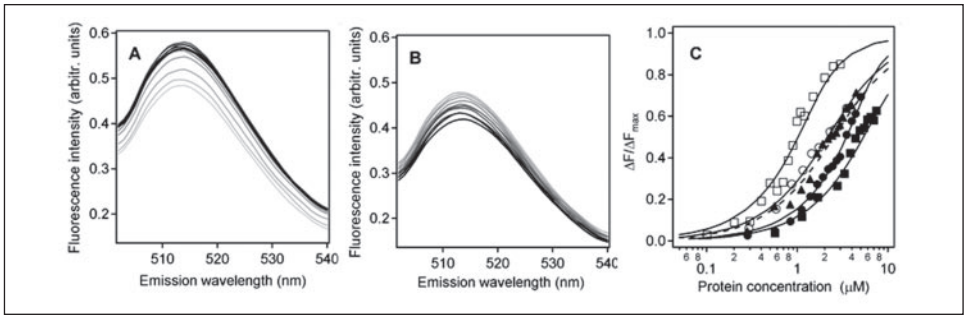

FIGURE 4. **Quantitative characterization of binding of $hIBPLA_2$, $hIIAPLA_2$, their N-terminal peptides, and the chimeric N10IIA/IB PLA_2 to phospholipid membranes.** *A,* dependence of fluorescence emission spectra of FPE, incorporated at 2 mol % in large unilamellar vesicles (100 nm in diameter) containing 58 mol % POPC and 40 mol % POPG, on the concentration of $hIBPLA_2$. The *increasing darkness of lines* corresponds to increasing concentrations of $hIBPLA_2$, which are indicated in *C*. The buffer contained 10 mM Hepes, 1 mM NaN_3, 1 mM EGTA (pH 7.4). Excitation was at 490 nm. *B,* control experiments, in which buffer was added instead of PLA_2 to FPE-containing vesicles in order to determine the effect of sample dilution, which was used for correction of spectra in *A*. The *increasing darkness of spectra* corresponds to increasing sample dilution. Fluorescence spectra were measured using a 0.4-cm optical path length quartz cuvette. *C,* membrane binding isotherms for $hIBPLA_2$ (*open circles*), N10hIB peptide (*closed circles*), $hIIAPLA_2$, (*open squares*), N10hIIA peptide (*closed squares*), and the chimeric N10IIA/IB PLA_2 (*triangles*). Lipid composition of vesicles and the buffer are as in *A*. The relative increase in peak fluorescence intensity of FPE, $\Delta F/\Delta F_{max}$, is plotted against protein concentration. The theoretical isotherms are simulated through Equations 3 and 4, using the binding parameters (K_D and N) summarized in TABLE ONE; all lines are continuous except for that describing the binding of the chimeric PLA_2 (*broken line*).

zwitterionic PC membranes and tight binding to anionic membranes (48–50). For example, binding of human or snake group IIA PLA_2s to phospholipid membranes could only be detected in the presence of ≥15 mol % acidic lipid in membranes, such as DPPG or POPG (49, 50). Correspondingly, the activity of $hIIAPLA_2$ against phosphatidylcholine vesicles is 1000–10,000-fold lower than against phosphatidylglycerol vesicles (30, 49, 51). The dissociation constant of group IIA PLA_2 for zwitterionic membranes is in the millimolar range (48, 50, 52). Mammalian group IB PLA_2s also exhibit poor binding to zwitterionic membranes and low activity compared with membranes containing anionic lipids (30). Involvement of a large electrostatic factor in membrane binding of group I and II PLA_2s is a physiologically intrinsic feature of these enzymes. Our binding experiments indicated that not only group IB and IIA PLA_2s but also their N-terminal peptides did not bind to pure phosphatidylcholine membranes but did bind to membranes containing acidic lipid. Given all these circumstances, and the fact that most biological membranes have surface charge corresponding to 20 ± 5% anionic lipids (53, 54), we used membranes containing 20% anionic lipid in binding experiments. We also used membranes containing 40% anionic lipid in order to determine the sensitivity of membrane binding of all five molecules to the membrane surface charge (binding isotherms are only shown for vesicles with 40% POPG in Fig. 4*C*). Parameters K_D and N for the binding of all five molecules to membranes containing 20 and 40 mol % POPG are summarized in TABLE ONE. The data indicate that $hIIAPLA_2$ and the N10hIB peptide exhibit tighter binding to membranes containing 20 mol % POPG (K_D = 2.5–2.8 μM) and 40 mol % POPG (K_D = 0.3–0.6 μM) compared with the other molecules. The membrane binding affinity of $hIIAPLA_2$ (in terms of K_D) undergoes an ~10-fold increase upon increasing the content of negative lipid in membranes from 20 to 40 mol %. The sensitivity of membrane binding affinity to the membrane negative surface charge decreases in the sequence: $hIIAPLA_2$ > N10IIA/IB ≥ $hIBPLA_2$ ≥ N10hIB > N10hIIA. In order to interpret these characteristics, the pI values and the excess charge of the molecules, as shown in TABLE ONE, should be taken into account. There is some, but inconsistent, correlation between the affinities for anionic membranes and pI values of the molecules. The N10hIB peptide, which has three cationic and no anionic residues (the C-terminal carboxyl group is suggested to be compensated by the N-terminal amino group), has the highest pI value and relatively high membrane binding affinity but lower sensitivity to the membrane anionic charge than the $hIIAPLA_2$ and the chimeric protein. It is very likely that the binding of proteins and peptides to anionic membranes is determined not only by the pI values but, perhaps more importantly, by the actual excess cationic charge of the molecule. For example, the $hIIAPLA_2$ has much higher excess positive charge than any of the molecules studied, which results in strong binding to anionic membranes and high sensitivity to the membrane surface charge. The chimeric protein, on the other hand, has only ~1.2 excess cationic charge at pH 7.4, resulting in weaker membrane binding, especially at 20 mol % of acidic lipid in membranes, and lower sensitivity to the membrane anionic charge.

The data of TABLE ONE indicate that membrane binding capabilities of PLA_2s are not additive in terms of such capabilities of their constituent parts. The dissociation constants for the $hIBPLA_2$ fragment ΔN10 that lacks the first 10 residues was determined previously to be 29 and 18.5 μM for membranes containing 20 and 40 mol % POPG, which correspond to the binding energies of −8.56 and −8.83 kcal/mol, respectively (13). On the other hand, the respective membrane binding energies of the N10hIIA peptide are −9.52 and −10 kcal/mol (TABLE ONE). If the membrane binding energy of the chimeric N10IIA/IB PLA_2 was additively determined by those of the ΔN10 fragment and the N10hIIA peptide, then the chimeric protein would bind to membranes with ΔG_b = −18 to −19 kcal/mol, whereas the experimentally measured values are only −9.2 to −10.2 kcal/mol. This is similar to earlier findings that the membrane binding energy of the full-length $hIBPLA_2$ was only ~50% of the sum of binding energies of the ΔN10 fragment and the N10hIB peptide (13). Apparently, the functional role of the N-terminal peptide of PLA_2, which is absolutely required for the enzyme activity (13), is not strengthening the membrane binding affinity but rather is to facilitate a productive mode binding of the enzyme to the membrane surface.

Positioning the Chimeric PLA_2 at the Membrane Surface—Previously, we have determined the precise positioning of $hIBPLA_2$ on phospholipid membranes (18), and we have shown that the N-terminal α-helix is a crucial determinant for the productive mode membrane binding of the enzyme (13). In order to understand the effect of the substitution of the N-terminal α-helix on the membrane binding mode of PLA_2, here we have studied the angular orientation of the membrane-bound chimeric N10IIA/IB PLA_2. Because our task was to achieve the structure of the membrane-bound protein at atomic details, first we determined the structure of the chimeric PLA_2 by the internet-based server Swiss-Model (24), using the structure of the porcine pancreatic PLA_2 as a template. The obtained structure revealed three α-helices. The C-α atom coordinates of the three helices were used to determine the interhelical angles, η_{12} = 35.5°, η_{13} = 36.6°, and η_{23} = 6.2°, where η_{ij} is the

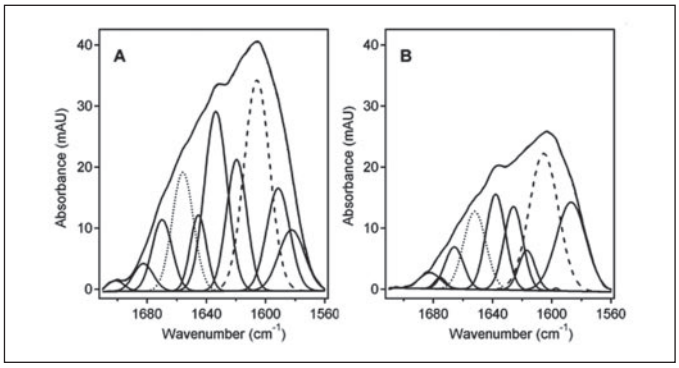

FIGURE 5. **Determination of the angular orientation of the membrane-bound segmentally ^{13}C-labeled chimeric N10IIA/IB PLA_2 by polarized ATR-FTIR spectroscopy.** The composition of the supported phospholipid bilayer and the method of sample preparation are the same as in Fig. 3. The segmentally ^{13}C-labeled N10IIA/IB PLA_2 was dissolved in an H_2O-based buffer of 100 mM NaCl, 1 mM NaN_3, 1 mM EGTA, 50 mM Hepes (pH 7.4) and injected into the cell containing the supported membrane. After allowing the protein to bind to the membrane (~15 min), the cell was flushed with a similar buffer prepared in ^2H_2O, and ATR-FTIR spectra were recorded at parallel (*A*) and perpendicular (*B*) polarizations of the infrared light. Amide I components were generated by curve fitting, using the second derivatives for resolution enhancement. Amide I components corresponding to the N-terminal unlabeled α-helix (*dotted line*) and the two ^{13}C-labeled α-helices (*dashed line*) are located at 1657–1654 and at 1608–1604 cm^{-1}, respectively. The sum of all components is shown by *dashed-dotted line*, which nearly coincides with the measured amide I contour.

angle between helices *i* and *j*. The fact that the helices 2 and 3 are nearly parallel to each other allowed us to use a common order parameter for these two helices in terms of their spatial orientation.

The next step was to determine the orientations of the unlabeled helix 1 and ^{13}C-labeled helices 2 and 3 with respect to the membrane normal for the membrane-bound chimeric PLA_2, which was achieved by polarized ATR-FTIR experiments. Fig. 5 shows the curve-fitted amide I spectra of the membrane-bound protein at parallel and perpendicular polarizations.

The intensities of polarized amide I components for the N-terminal helix and for the ^{13}C-labeled helices 2 and 3, which were spectrally resolved because of an ~50 cm^{-1} downshift of the signal from the ^{13}C-labeled helices, were used to evaluate the respective dichroic ratios as $R_{\alpha 1} = 1.45 \pm 0.08$ and $R_{\alpha 2,3} = 1.35 \pm 0.05$, where the subscripts indicate the corresponding α-helices (shown are mean values and standard deviations obtained from curve fitting of several polarized amide I spectra). The mean values of dichroic ratios yield the order parameters of $S_{\alpha 1} = -0.268$ for the helix 1 and $S_{\alpha 2,3} = -0.392$ for the helices 2 and 3, with ranges of variation from -0.183 to -0.368 and from -0.331 to -0.457, respectively. Interpretation of these uncertainties in terms of angular orientation indicates that the amplitude of wobbling of the helices relative to the membrane normal does not exceed 10°, which is reasonable regarding the fluid nature of the membrane. Thus, the ATR-FTIR measurements provide the helical orientations with respect to the membrane with an acceptable degree of accuracy. The order parameters were used to find the average tilt angles of the respective helix axis relative to the membrane normal, $\langle \cos\theta_{\alpha 1} \rangle = 0.394$ and $\langle \cos\theta_{\alpha 2,3} \rangle = 0.268$. At this point, we had the orientations of all helices in the protein coordinate system, Σ_p, and their orientations relative to the membrane normal (the *z* axis). This allowed expression of $\cos\theta_{\alpha 1}$ and $\cos\theta_{\alpha 2,3}$ through the cosines of angles between helical axes and the axes of the protein system $\Sigma_p$and the cosines of angles between the *z* axis and the axes of the coordinate system Σ_p, cos(zx*), cos(*zy**), and cos(*zz**), assuming these two coordinate systems are brought to a common origin (see Ref. 18 for details). Combination of these with the law of direction cosines: $\cos^2(zx^*) + \cos^2(zy^*) + \cos^2(zz^*) = 1$, allowed determination of $\cos(zx^*) = -0.392$, $\cos(zy^*) = -0.158$, and $\cos(zz^*) = 0.906$. These three cosines determine the angular orientation of the protein relative to the membrane normal.

In order to determine the structure of the membrane-bound protein, *i.e.* the protein atom coordinates in the membrane coordinate system Σ_m, the remaining six angles between the axes of the coordinate systems Σ_m and Σ_p are also required. Because the membrane is only anisotropic in the vertical dimension (the *z* axis) but is isotropic in the lateral dimension (the *x* and *y* axes), the protein has a rotational freedom about the *z* axis but not the *x* or the *y* axes. Therefore, all azimuthal orientations of the protein, *i.e.* all angles of rotation about the *z* axis, are equivalent. This allowed us to select arbitrarily one of the six angles, *e.g.* $\cos(yx^*) = 0.456$, and use the laws of direction cosines to determine the remaining angles. Thus, we obtained all nine angles between the axes of the coordinate systems Σ_m and Σ_p: $\cos(zx^*) = -0.392$, $\cos(zy^*) = -0.158$, and $\cos(zz^*) = 0.906$, $\cos(yx^*) = 0.456$, $\cos(yy^*) = 0.822$, $\cos(yz^*) = 0.341$, $\cos(xx^*) = -0.799$, $\cos(xy^*) = 0.547$, $\cos(xz^*) = -0.250$. These nine cosines were used to transform the protein atom coordinates from the protein system Σ_p to the membrane system Σ_m, assuming the two systems have a common origin.

The above operations only provide the angular orientation of the protein relative to the membrane. The vertical location of the protein relative to the membrane plane is still required to position the protein on the membrane. This can be determined by membrane depth-dependent fluorescence quenching of a protein-bound fluorophore by lipids that contain quenchers at various positions of hydrocarbon chains. We have determined previously the depth of insertion of $hIBPLA_2$ into POPC/POPG membranes by this method (18). Although $hIBPLA_2$ is an appropriate protein for this purpose because it has a single tryptophan at position 3, which is a part of the membrane binding face, this is not the case with the chimeric N10IIA/IB PLA_2 because this molecule is devoid of tryptophans. Although other native fluorophores, such as tyrosines, can also be used for quenching experiments, the abundance of tyrosines in N10IIA/IB PLA_2 prevents any meaningful interpretation of the fluorescence quenching data in terms of the depth of membrane insertion. Therefore, we used the information regarding membrane insertion of $hIBPLA_2$ in order to locate the chimeric N10IIA/IB PLA_2 along the membrane normal. For the $hIBPLA_2$, the geometric center of the indole ring of Trp^3 was located at 9 Å from the membrane center (18). By assuming insertion of the chimeric N10IIA/IB PLA_2 into the membrane to a similar depth, and by taking into consideration the difference in size between Trp and Val, we positioned the side chain of Val^3 of the chimeric protein at 10 Å from the membrane center. This was done by adjusting the *z* coordinates of all atoms of the protein so the *z* coordinate of the geometric center of Val^3 was 10 Å, whereas the angular orientation of the protein with respect to the membrane was maintained as determined above. These procedures resulted in a model for the structure of the membrane-bound chimeric N10IIA/IB PLA_2, which is shown in Fig. 6*A*. In Fig. 6, *A* and *B*, three planes of atoms are introduced that are perpendicular to the membrane normal and schematically identify the locations of terminal methyl carbons of the acyl chains of glycerophospholipids (membrane center), the *sn*-1 carbonyl oxygens, and the phosphorus atoms of lipid phosphate groups. The *z* coordinates of these three planes are $z = 0$, $z = 14.5$ Å, and $z = 20$ Å, respectively, which is based on x-ray diffraction data on POPC bilayers (55).

The structure of the membrane-bound N10IIA/IB PLA_2, which we refer to as the quinary structure of a membrane protein (18), is consistent with previously reported models of membrane anchoring of the group I/II PLA_2s (8, 56–58), with one important difference, *i.e.* the depth of membrane insertion of the protein. Although penetration of secretory PLA_2s into membranes has not been reported by others, we

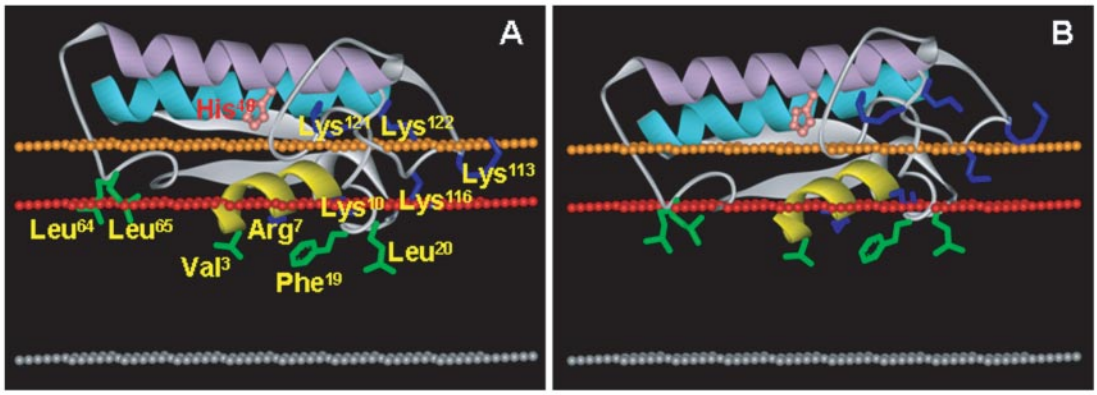

FIGURE 6. **Model for membrane-bound chimeric N10IIA/IB PLA$_2$ obtained by homology modeling, polarized ATR-FTIR spectroscopy, and analytical geometry algorithms.** The structure in *A* was obtained by using the mean values of dichroic ratios of the unlabeled N-terminal α-helix and of the two ^{13}C-labeled α-helices. The structure of PLA$_2$ was homology-modeled by Swiss-Model using porcine pancreatic PLA$_2$ structure (Protein Data Bank entry 1P2P) as a template. The protein is presented in a ribbon format, with the α-helices 1–3 colored *yellow, purple,* and *light blue,* respectively. The side chains of amino acids directly involved in physical interactions with the membrane are shown in a *stick format*; hydrophobic residues are shown in *green* and the cationic residues in *blue*. The catalytic His^{48} is shown in *ball-and-stick format* and colored *rose*. The three layers of nonprotein atoms are introduced to schematically show membrane sections corresponding to the acyl chain terminal methyl carbons (*gray*), the *sn*-1 carbonyl oxygens (*red*), and the phosphorus atoms (*orange*) of membrane glycerophospholipids. The *z*-coordinates of these layers are 0, 14.5, and 20 Å, respectively. The whole structure is turned about the *z* axis by 10° and slightly (~1°) about the *y* axis. Without these rotations, the plane of the picture would correspond to the *yz* plane. *B,* the protein has been rotated by 10° about an axis parallel to the *x* axis, which results in immersion of Leu^{64} and Leu^{65} into the hydrophobic part of the membrane.

have documented insertion of hIBPLA$_2$ into POPC/POPG membrane to a depth of ~9 Å from the membrane center (18), which is the basis for positioning the chimeric PLA$_2$ relative to the membrane surface as shown in Fig. 6. The mode of membrane binding of the chimeric PLA$_2$ resembles that of the hIBPLA$_2$ (18). In both cases, the α-helices 2 and 3 are tilted by ~75° from the membrane normal toward the membrane surface. The N-terminal α-helix is oriented obliquely relative to the membrane plane and is by ~7° more tangential in the chimeric PLA$_2$ than in hIBPLA$_2$. As shown below, the membrane-bound N10hIIA peptide also turned out to be oriented more laterally on the membrane surface compared with the N10hIB peptide, implying that the orientation of the membrane-bound PLA$_2$ is probably affected by the intrinsic properties of the N-terminal helix. Membrane binding of the protein is stabilized by hydrophobic, ionic, and H-bonding interactions. In Fig. 6*A*, the cationic side chains of Arg^7, Lys^{10}, and Lys^{116} are located at the level of the hydrophobic/polar interface of the membrane and are very likely to be involved in H-bonding with lipid carbonyl oxygens. Side chains of other three lysines (residues 113, 121, and 122) are at the level of lipid phosphate groups and are likely engaged in ionic contacts with those groups. Side chains of three nonpolar residues, Val^3, Phe^{19}, and Leu^{20}, act as hydrophobic anchors for the PLA$_2$-membrane interaction. In this particular orientation, a hydrophobic spot of the protein, marked by Leu^{64} and Leu^{65}, is in the polar region of the ester carbonyl groups of membrane lipids. Because the model of Fig. 6*A* presents an enzyme bound to a membrane in the fluid phase rather than a rigid, immobile structure, the protein is likely to have some degree of motional flexibility, including the angular orientation. The above estimates of the helical order parameters, which are the basis for orientation determination, indicated that within the accuracy of the measurements the orientation of PLA$_2$ can fluctuate within the limits of ~10°. Rotation of PLA$_2$ by 10° about an axis parallel to the *x* axis and passing through the center of the protein molecule results in a structure presented in Fig. 6*B*. This seems to be a viable structure because it is still close to the limits of experimental error and maintains the characteristic features of the structure obtained using the average values of helical order parameters (Fig. 6*A*). In this structure, the side chains of Leu^{64} and Leu^{65} are conveniently embedded in the hydrocarbon chain region of the membrane, which stabilizes the membrane binding of PLA$_2$. This is in accord with earlier indications that the loop containing these leucines is a part of interfacial binding region of group IB PLA$_2$s (9, 56) that is involved in conformational changes in the enzyme upon interfacial activation (8). On the other hand, in this model Lys^{121} and Lys^{122}, which form ionic bonds with the lipid phosphate groups in the structure of Fig. 6*A*, are moved farther away from the membrane surface. Also, the residues Lys^{113} and Lys^{116} are located in a less energetically favorable manner than in the model of Fig. 6*A*. These considerations lead to an inference that the actual membrane binding mode of the protein is likely to be between the two models presented in Fig. 6. It is also possible that PLA$_2$ undergoes transitions between distinct orientations during the catalytic process.

In order to determine whether the difference in the orientations of membrane-bound hIBPLA$_2$ and the chimeric N10IIA/IB PLA$_2$, *i.e.* the more horizontal orientation of the N-terminal helix of the chimeric protein relative to the membrane plane, is dictated by the intrinsic properties of the N-terminal peptides of group IB and IIA PLA$_2$s, we evaluated the orientations of the peptides bound to supported membranes by polarized ATR-FTIR. The amide I spectra of the N10hIIA peptide at parallel and perpendicular orientations of the incident light were curve-fitted using the frequencies of four components identified by second derivatives (Fig. 7). The α-helical components, which were centered between 1653 and 1651 cm^{-1}, were used to evaluate the helical content in the membrane-bound peptide and its orientation. The helical content was estimated as $f_\alpha = (A_{\alpha,\parallel} + 0.8A_{\alpha,\perp})/(A_\parallel + 0.8A_\perp) = 46\%$, where $A_{\alpha,\parallel}$ and $A_{\alpha,\perp}$ are the areas of α-helical components, whereas $A_\parallel$ and $A_\perp$ are the total amide I areas at the respective polarizations. This implies that the membrane-bound N10hIIA peptide itself attains only partial α-helicity, meaning that the helical conformation of the N terminus in the full-length PLA$_2$ is facilitated by interactions with the rest of the protein. Most interestingly, the N10hIB peptide was previously shown to contain ~70% α-helix when bound to supported POPC/POPG membranes (13). This suggests that the N-terminal domain of the hIBPLA$_2$ has a stronger helical propensity and forms more stable, or rigid, helices than the N terminus of the hIIAPLA$_2$, consistent with earlier findings discussed in the Introduction and with the data of this work. The α-helical dichroic ratio of the N10hIIA peptide was $A_{\alpha,\parallel}/A_{\alpha,\perp} = 1.34$, and the order parameter was −0.41, corresponding to a tilt angle relative to the membrane normal of ~76°. For comparison, the tilt angle of the

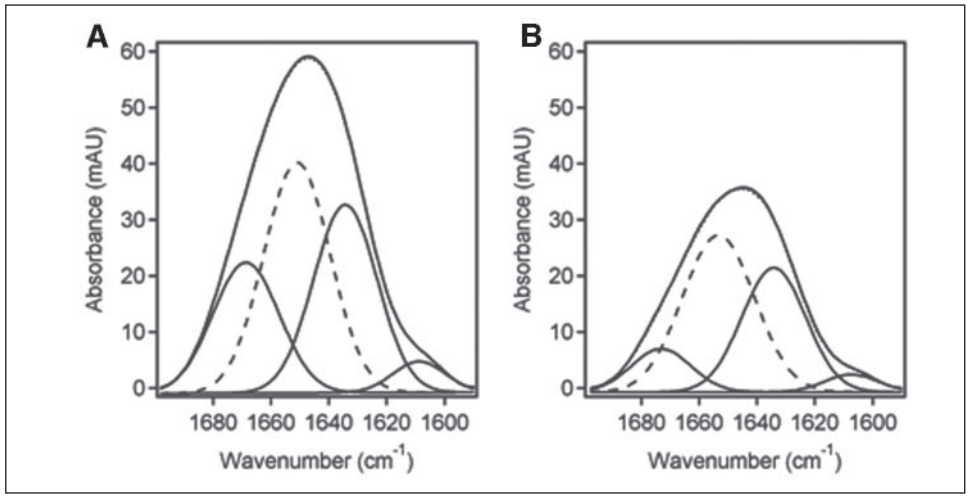

FIGURE 7. **Determination of the secondary structure and orientation of the membrane-bound N-terminal peptide of the group IIA PLA_2 by ATR-FTIR spectroscopy.** Curve-fitted amide I spectra of the membrane-bound N10hIIA peptide measured by ATR-FTIR spectroscopy at parallel (*A*) and perpendicular (*B*) polarizations of the infrared light. The peptide is bound to supported membranes composed of POPC and POPG, as described in Fig. 3, in the same buffer. Curve fitting is based on the frequencies of four components, identified by the second derivatives. The components shown in *dashed lines* are assigned to α-helix. The sums of all four components are shown in *dotted lines*, which can hardly be seen because they coincide with measured spectra.

N10hIB peptide was estimated to be ~64° (13). These data suggest that the N-terminal helix of the hIIAPLA$_2$ binds to the membrane with a more horizontal orientation than that of hIBPLA$_2$. Given the larger tilt angle of the N-terminal helix of the chimeric N10IIA/IB PLA$_2$ compared with that of hIBPLA$_2$, these findings suggest that the mode of membrane binding of PLA$_2$ is affected by the intrinsic properties of the N-terminal helix. Because the hydrophobic face of the amphipathic N-terminal α-helix forms a wall for the substrate-binding pocket of PLA$_2$ (6, 56), the orientation of the helix relative to the membrane plane is likely to control the enzyme-substrate interaction step of the catalytic reaction, again indicating a regulatory role of the N-terminal helix in PLA$_2$ function.

Determination of the membrane binding mode of a protein as described in this work provides the structure of the proteins in which the *z* coordinate of each atom is the distance from the membrane center. The quinary structure of a membrane protein offers an unprecedented opportunity to immediately determine the location of every single amino acid residue, and each atom, relative to the structural moieties of membrane lipids. In the models of Fig. 6, the entrance of the phospholipid substrate into the catalytic pocket of the membrane-bound enzyme is between the N-terminal helix and the highlighted His^{48} and is flanked by two loops from the left and the right. The *z* coordinates of the imidazole nitrogens of the catalytic His^{48}, which is located just slightly above the membrane surface, are 22.6 Å. Considering that the *sn*-2 ester groups of POPC and 1,2-dioleoyl-*sn*-glycero-3-phosphocholine are at ~15.5 Å from the membrane center (55, 59), the phospholipid molecule has to travel only ~7 Å in order to reach the catalytic center of the enzyme, in contrast to the earlier conjectures assuming an ~15 Å distance between the catalytic center of membrane-bound PLA$_2$ and the lipid cleavage site (6–8, 56, 58).

Conclusions—As a logical development of the previous findings that the N-terminal α-helix of PLA$_2$ acts as a structural determinant for the productive mode membrane binding and activation of the enzyme (13), in this study we assess the effects of substitution of the N-terminal helix of human group IB PLA$_2$ by that of the group IIA PLA$_2$ on membrane binding properties and membrane-induced conformational changes in PLA$_2$. The chimeric PLA$_2$ reveals conformational features that are different from those of hIBPLA$_2$ and hIIAPLA$_2$ and has severalfold lower activity compared with both hIBPLA$_2$ and hIIAPLA$_2$. Although the N-terminal helix of membrane-bound hIBPLA$_2$ has a more rigid structure than the other helices, the structure of the chimeric PLA$_2$ is more rigid compared with both hIBPLA$_2$ and hIIAPLA$_2$, but the N-terminal helix in the chimeric protein is flexible. The present data and earlier data allow construction of a model for the membrane-bound chimeric PLA$_2$, including the angular orientation and depth of membrane insertion. The orientation of the N-terminal helix of the chimeric PLA$_2$ is more horizontal relative to the membrane surface compared with the hIBPLA$_2$, which reflects the intrinsic membrane-binding properties of the N10hIB and N10hIIA peptides. Membrane binding data indicate that the binding affinity of N10IIA/IB PLA$_2$ for anionic membranes was 4–6 times weaker than that of hIIAPLA$_2$ and was comparable with that of hIBPLA$_2$, implying that the N-terminal α-helix is not as important in the membrane binding strength of hIIAPLA$_2$ as it is for hIBPLA$_2$. In the case of hIIAPLA$_2$, which carries a tremendous excess cationic charge, membrane binding is primarily driven by electrostatic interactions, impeding binding to zwitterionic membranes and facilitating binding to anionic membranes. In the case of hIBPLA$_2$ that carries only a moderate overall excess charge, the N-terminal helix is a major determinant of the membrane binding properties by virtue of three cationic charges and Trp^3. The N-terminal helix of group IB PLA$_2$s seems to be a unique tool that plays a critical role in membrane binding and subsequent activation of the enzymes. Somewhat surprisingly, the N-terminal helix of hIIAPLA$_2$, which has only two cationic residues and no Trp^3, turns out to support substantial activity and a productive membrane binding mode when substituted into hIBPLA$_2$. These data provide evidence that the N-terminal helix of PLA$_2$s is an indispensable but substitutable domain in terms of supporting the proper membrane binding mode and activity of the enzymes.

REFERENCES

1. Six, D. A., and Dennis, E. A. (2000) *Biochim. Biophys. Acta* **1488,** 1–19
2. Murakami, M., and Kudo, I. (2004) *Biol. Pharm. Bull.* **27,** 1158–1164
3. Masuda, S., Murakami, M., Komiyama, K., Ishihara, M., Ishikawa, Y., Ishii, T., and Kudo, I. (2005) *FEBS J.* **272,** 655–672
4. Scott, D. L., and Sigler, P. B. (1994) *Adv. Protein Chem.* **45,** 53–88
5. Arni, R. K., and Ward, R. J. (1996) *Toxicon* **34,** 827–841
6. Berg, O. G., Gelb, M. H., Tsai, M. D., and Jain, M. K. (2001) *Chem. Rev.* **101,** 2613–2654
7. Pan, Y. H., Epstein, T. M., Jain, M. K., and Bahnson, B. J. (2001) *Biochemistry* **40,** 609–617
8. Bahnson, B. J. (2005) *Arch. Biochem. Biophys.* **433,** 96–106
9. Jain, M. K., and Maliwal, B. P. (1993) *Biochemistry* **32,** 11838–11846
10. Maliwal, B. P., Yu, B. Z., Szmacinski, H., Squier, T., van Binsbergen, J., Slotboom, A. J., and Jain, M. K. (1994) *Biochemistry* **33,** 4509–4516
11. van den Berg, B., Tessari, M., Boelens, R., Dijkman, R., de Haas, G. H., Kaptein, R., and Verheij, H. M. (1995) *Nat. Struct. Biol.* **2,** 402–406
12. van den Berg, B., Tessari, M., Boelens, R., Dijkman, R., Kaptein, R., de Haas, G. H., and Verheij, H. M. (1995) *J. Biomol. NMR* **5,** 110–121
13. Qin, S., Pande, A. H., Nemec, K. N., and Tatulian, S. A. (2004) *J. Mol. Biol.* **344,** 71–89
14. Jerala, R., Almeida, P. F. F., Ye, Q., Biltonen, R. L., and Rule, G. S. (1996) *J. Biomol.*

NMR **7,** 107–120
15. Tatulian, S. A., Biltonen, R. L., and Tamm, L. K. (1997) *J. Mol. Biol.* **268,** 809–815
16. Tatulian, S. A. (2001) *Biophys. J.* **80,** 789–800
17. Tatulian, S. A. (2003) *Biophys. J.* **84,** 1773–1783
18. Tatulian, S. A., Qin, S., Pande, A. H., and He, X. (2005) *J. Mol. Biol.* **351,** 939–947
19. Othman, R., Baker, S., Li, Y., Worrall, A. F., and Wilton, D. C. (1996) *Biochim. Biophys. Acta* **1303,** 92–102
20. Wall, J., Golding, C. A., Van Veen, M., and O'Shea, P. (1995) *Mol. Membr. Biol.* **12,** 183–192
21. Golding, C., Senior, S., Wilson, M. T., and O'Shea, P. (1996) *Biochemistry* **35,** 10931–10937
22. Marsh, D. (1999) *Biophys. J.* **77,** 2630–2637
23. Tatulian, S. A. (2003) *Biochemistry* **42,** 11898–11907
24. Schwede, T., Kopp, J., Guex, N., and Peitsch, M. C. (2003) *Nucleic Acids Res.* **31,** 3381–3385
25. Donato, H., Jr., Mani, R. S., and Kay, C. M. (1991) *Biochem. J.* **276,** 13–18
26. Ruan, K., Li, J., Liang, R., Xu, C., Yu, Y., Lange, R., and Balny, C. (2002) *Biochem. Biophys. Res. Commun.* **293,** 593–597
27. Cooper, T. M., and Woody, R. W. (1990) *Biopolymers* **30,** 657–676
28. Zhou, N. E., Kay, C. M., and Hodges, R. S. (1992) *J. Biol. Chem.* **267,** 2664–2670
29. Sreerama, N., Venyaminov, S. Y., and Woody, R. W. (1999) *Protein Sci.* **8,** 370–380
30. Baker, S. F., Othman, R., and Wilton, D. C. (1998) *Biochemistry* **37,** 13203–13211
31. Beers, S. A., Buckland, A. G., Giles, N., Gelb, M. H., and Wilton, D. C. (2003) *Biochemistry* **42,** 7326–7338
32. Huang, R., Kubelka, J., Barber-Armstrong, W., Silva, R. A. G. D., Decatur, S. M., and Keiderling, T. A. (2004) *J. Am. Chem. Soc.* **126,** 2346–2354
33. Moran, A., and Mukamel, S. (2004) *Proc. Natl. Acad. Sci. U. S. A.* **101,** 506–510
34. Paul, C., and Axelsen, P. H. (2005) *J. Am. Chem. Soc.* **127,** 5754–5755
35. Paul, C., Wang, J., Wimley, W. C., Hochstrasser, R. M., and Axelsen, P. H. (2004) *J. Am. Chem. Soc.* **126,** 5843–5850
36. Krimm, S., and Bandekar, J. (1986) *Adv. Protein Chem.* **38,** 181–364
37. Jackson, M., and Mantsch, H. H. (1995) *Crit. Rev. Biochem. Mol. Biol.* **30,** 95–120
38. Venyaminov, S. Y., Hedstrom, J. F., and Prendergast, F. G. (2001) *Proteins* **45,** 81–89
39. Heimburg, T., Schuenemann, J., Weber, K., and Geisler, N. (1996) *Biochemistry* **35,** 1375–1382
40. Reisdorf, W. C., and Krimm, S. (1996) *Biochemistry* **35,** 1383–1386
41. Cohen, C., and Parry, D. A. (1994) *Science* **263,** 488–489
42. Pastrana-Rios, B. (2001) *Biochemistry* **40,** 9074–9081
43. Barber-Armstrong, W., Donaldson, T., Wijesooriya, H., Silva, R. A. G. D., and Decatur, S. M. (2004) *J. Am. Chem. Soc.* **126,** 2339–2345
44. Némethy, G., Phillips, D. C., Leach, S. J., and Scheraga, H. A. (1967) *Nature* **214,** 363–365
45. Rothschild, K. J., and Clark, N. A. (1979) *Science* **204,** 311–312
46. Krimm, S., and Dwivedi, A. M. (1982) *Science* **216,** 407–408
47. Barnett, S. M., Edwards, C. M., Butler, I. S., and Levin, I. W. (1997) *J. Phys. Chem.* **101,** 9421–9424
48. Gelb, M. H., Cho, W., and Wilton, D. C. (1999) *Curr. Opin. Struct. Biol.* **9,** 428–432
49. Bezzine, S., Bollinger, J. G., Singer, A. G., Veatch, S. L., Keller, S. L., and Gelb, M. H. (2002) *J. Biol. Chem.* **277,** 48523–48534
50. Gadd, M. E., and Biltonen, R. L. (2000) *Biochemistry* **39,** 9623–9631
51. Han, S. K., Kim, K. P., Koduri, R., Bittova, L., Munoz, N. M., Leff, A. R., Wilton, D. C., Gelb, M. H., and Cho, W. (1999) *J. Biol. Chem.* **274,** 11881–11888
52. Han, S. K., Yoon, E. T., Scott, D. L., Sigler, P. B., and Cho, W. (1997) *J. Biol. Chem.* **272,** 3573–3582
53. Surette, M. E., and Chilton, F. H. (1998) *Biochem. J.* **330,** 915–921
54. D'Antuono, C., Fernandez-Tome, M. C., Sterin-Speziale, N., and Bernik, D. L. (2000) *Arch. Biochem. Biophys.* **382,** 39–47
55. McIntosh, T. J., and Holloway, P. W. (1987) *Biochemistry* **26,** 1783–1788
56. Yu, B. Z., Janssen, M. J. W., Verheij, H. M., and Jain, M. K. (2000) *Biochemistry* **39,** 5702–5711
57. Canaan, S., Nielsen, R., Ghomashchi, F., Robinson, B. H., and Gelb, M. H. (2002) *J. Biol. Chem.* **277,** 30984–30990
58. Liu, X., Zhu, H., Huang, B., Rogers, J., Yu, B. Z., Kumar, A., Jain, M. K., Sundaralingam, M., and Tsai, M. D. (1995) *Biochemistry* **34,** 7322–7324
59. Hristova, K., Wimley, W. C., Mishra, V. K., Anantharamiah, G. M., Segrest, J. P., and White, S. H. (1999) *J. Mol. Biol.* **290,** 99–117

Evidence for the Regulatory Role of the N-terminal Helix of Secretory Phospholipase A_2 from Studies on Native and Chimeric Proteins

Shan Qin, Abhay H. Pande, Kathleen N. Nemec, Xiaomei He and Suren A. Tatulian

J. Biol. Chem. 2005, 280:36773-36783.
doi: 10.1074/jbc.M506789200 originally published online August 15, 2005
